

MR. DANIEL NAJAFALI (Orcid ID : 0000-0003-1509-9229)
MR. ROBERT PERTTILÄ (Orcid ID : 0000-0001-8030-7077)
PROF. HUANG-CHIAO HUANG (Orcid ID : 0000-0002-5406-0733)

Article type : Special Issue Research Article

Predictors and Limitations of the Penetration Depth of Photodynamic Effects in the Rodent Brain[†]

Collin T. Inglut^{1,+}, Brandon Gaitan^{1,+}, Daniel Najafali¹, Irati Abad Lopez¹, Nina P. Connolly^{2,3}, Seppo Orsila⁴, Robert Perttilä⁴, Graeme F. Woodworth^{2,3}, Yu Chen^{1,2}, Huang-Chiao Huang^{1,2*}

¹Fischell Department of Bioengineering, University of Maryland, College Park, MD 20742, USA

²Marlene and Stewart Greenebaum Cancer Center, University of Maryland School of Medicine, Baltimore, MD 21201, USA

³Department of Neurosurgery, University of Maryland School of Medicine, Baltimore, MD 21201, USA

⁴Modulight, Inc., Hermiankatu 22, FI-33720, Tampere, Finland

⁺These authors contributed equally to this work

***Corresponding author's email:** hchuang@umd.edu (Huang-Chiao Huang)

[†]This article is part of a Special Issue dedicated to Dr. Jarod Finlay.

This article has been accepted for publication and undergone full peer review but has not been through the copyediting, typesetting, pagination and proofreading process, which may lead to differences between this version and the Version of Record. Please cite this article as doi: 10.1111/php.13155

This article is protected by copyright. All rights reserved.

ABSTRACT

Fluorescence-guided surgery (FGS) is routinely utilized in clinical centers around the world, whereas the combination of FGS and photodynamic therapy (PDT) has yet to reach clinical implementation and remains an active area of translational investigations. Two significant challenges to the clinical translation of PDT for brain cancer are: 1) Limited light penetration depth in brain tissues, and 2) Poor selectivity and delivery of the appropriate photosensitizers. To address these shortcomings, we developed nanoliposomal protoporphyrin IX (Nal-PpIX) and nanoliposomal benzoporphyrin derivative (Nal-BPD), and then evaluated their photodynamic effects as a function of depth in tissue and light fluence using rat brains. Although red light penetration depth (defined as the depth at which the incident optical energy drops to $1/e$, ~37%) is typically a few millimeters in tissues, we demonstrated that the remaining optical energy could induce PDT effects up to 2 cm within brain tissues. Photobleaching and singlet oxygen yield studies between Nal-BPD and Nal-PpIX suggest that deep-tissue PDT (>1 cm) is more effective when using Nal-BPD. These findings indicate that Nal-BPD-PDT is more likely to generate cytotoxic effects deep within the brain and allow for the treatment of brain invading tumor cells centimeters away from the main, resectable tumor mass.

Keywords: Photodynamic therapy; Light penetration depth; Benzoporphyrin derivative; Protoporphyrin IX; Nanoliposome

INTRODUCTION

Advancements in the study of light and optics have made significant impacts on neuroscience and modern medicine (1). A major output of this work has been the development of photodynamic therapy (PDT), now an emerging new tool in basic science and clinical practice (2-5). PDT is a photochemistry-based, non-thermal approach in which a biologically inert agent (i.e., photosensitizer) is transformed by the application of light at specific wavelengths into a cytotoxic therapeutic. This activation process occurs when the excited photosensitizer reacts with oxygen or other substrates to generate reactive molecular species (e.g., 1O_2 , H_2O_2 , $O_2^{\bullet-}$, $\bullet OH$) that kill or modulate cells and tissues. The fluorescent signal generated from the excited state photosensitizer can be harnessed for tumor imaging and

fluorescence-guided surgery (FGS) (6-8). In 2017, the US Food and Drug Administration (FDA) approved 5-aminolevulinic acid (5-ALA; Gleolan®) for use as an intraoperative imaging agent in patients with suspected high-grade gliomas (9). Upon excitation with ultraviolet/blue light (375-440 nm), gliomas that contain the 5-ALA-induced protoporphyrin IX (PpIX) emit a violet-red fluorescence, which can be readily visualized for surgical resection.

PDT is being evaluated in clinical trials for patients with brain cancer (e.g., NCT03048240, NCT03897491, NCT00003788, NCT01966809, NCT00002647, NCT01682746).

Glioblastoma (GBM) is the most common and lethal adult primary brain cancer, and the median patient survival continues to be less than 18 months despite major advancements in our understanding of GBM biology and efforts to develop new therapeutic strategies (10). A single PDT treatment has been shown to add up to 3-18 additional months to the lifespan of GBM patients (11). Optimized light delivery for effective PDT can be achieved through intraoperative, endoscopic, or balloon catheter-based fiber optics. The combination of FGS and PDT using different types of photosensitizers (e.g., benzoporphyrin derivative, 5-ALA, Photofrin®, temoporfin, hematoporphyrin derivative) have substantially improved survival outcomes in GBM patients (7). In a small-scale study, the mean survival of patients with GBM increased from 24.6 to 52.8 months when PDT was combined with FGS, compared to surgery alone (12). We and others now believe that the most advantageous and safe initial application of PDT is following tumor resection while in the operating room, prior to the administration of standard of care chemoradiation therapy (13). However, the long-term survival has not been achieved due in part to the limited light penetration in brain tissues, as well as the poor selectivity and delivery of the appropriate photosensitizers.

Tissue optical properties (i.e., absorption and scattering) influence light delivery and impact PDT outcomes (14). Red light penetration depth is typically 0.1-0.3 cm in tissues (1). This penetration depth is defined as the depth at which the incident optical energy drops to $1/e$ (~37%) (1). A number of *ex vivo* and *in silico* studies have already shown that the remaining 37% of photons can reach up to 2-5 cm deep in brain tissues (15-21). A series of studies by Wilson, Perria, and Cheng have shown that 630 nm light activation of hematoporphyrin derivative induces tumor necrosis and cell killing up to 0.8-1.5 cm deep within the brain tissue (22-24). On the other hand, Olzowy et al. demonstrated that 630 nm light activation (200 mW/cm^2) of 5-ALA-induced PpIX induces cerebral tissue damage only up to 0.4 cm

deep in the brain (25). Based on prior work showing that 690 nm light can penetrate approximately 40% further than 633 nm light in bladder tissue (26), here, we test if benzoporphyrin derivative (BPD) could be activated by 690 nm light at further depths within the brain tissue compared to using 635 nm light to activate PpIX.

Both BPD and PpIX have low water solubility (< 0.02 mg/mL) and cannot be directly injected intravenously. Aggregation of PpIX or BPD in their biological environment results in low bioavailability, heterogeneous biodistribution, and reduced PDT efficacy.

Nanoliposomes, composed of a hydrophobic lipid bilayer and an aqueous core, are the most studied and clinically used photosensitizer delivery vehicles (27, 4). In 2001, a polydisperse liposomal formulation of BPD (Visudyne®, 0.2-1 µm in diameter) was approved by the FDA for treatment of patients with wet age-related macular degeneration (28, 29). A clinical study using Visudyne®-PDT to treat patients with refractory brain tumors has also taken place (NCT00002647) (30). 5-ALA is a prodrug that can be preferentially converted into PpIX in cancerous cells due to decreased ferrochelatase activity and increased enzyme activity in the heme biosynthetic pathway compared to healthy tissue (31). While PpIX production in tumors is commonly achieved by the oral, topical, or systemic administration of 5-ALA (9), there has been a resurgence of interest in delivering exogenous PpIX. This is because the polar 5-ALA has limited diffusion through cell membranes and high doses of 5-ALA must be administered to reach clinically efficacious levels of PpIX (32-36). Using xenograft tumor models, Manivasager et al. showed that the tumor-to-normal tissue ratio (T/N ratio) of the 5-ALA-induced PpIX was 5-7 folds higher than that of exogenous PpIX (T/N ratio ~ 2) at 3-9 hours post tail vein injection (36). However, to induce a comparable fluorescence intensity of exogenous PpIX and 5-ALA-induced PpIX in the cancer cells, high doses of 250 mg/kg of 5-ALA has to be administered compared to using only 1 mg/kg of exogenous PpIX. Moreover, the delivery of exogenous PpIX using different nanoformulations (37-39) could potentially bypass the heterogeneous and low conversion of 5-ALA to PpIX observed in some tumors. Utsuki et al. demonstrated that 5-ALA-induced PpIX fluorescence in brain tumors was observed in 40 out of the 46 patients (34). Similarly, Walter and others have reported the sensitivity of 5-ALA-based photodynamic diagnosis is around 85% for detection of malignant tissues (40, 41). Based on these studies, here, we synthesized monodispersed nanoliposomal formulations of BPD (Nal-BPD) and PpIX (Nal-PpIX). Encapsulation within liposomes also provides the ability to perform a direct comparison between the two photosensitizers, where the majority of variables are held constant. Using Nal-BPD and Nal-

PpIX, we examined the limits of PDT as a function of tissue depth and light fluences in *ex vivo* rat brains, by monitoring the changes in photosensitizer photobleaching and singlet oxygen ($^1\text{O}_2$) production.

MATERIALS AND METHODS

Synthesis and characterization of Nal-BPD and Nal-PpIX. Nanoliposomes containing BPD or PpIX within its bilayer (Nal-BPD or Nal-PpIX) were synthesized via freeze-thaw extrusion as described previously (42-45, 48). Briefly, lipids, dipalmitoylphosphatidylcholine (DPPC), cholesterol, and distearoylphosphatidylethanolamine-methoxy polyethylene glycol (DSPE-PEG), and 1,2-dioleoyl-3-trimethylammonium-propane (DOTAP) (Avanti Polar Lipids), were co-dissolved with BPD (50 nmoles, U.S. Pharmacopeial) at 0.15 mol% BPD-to-lipid ratio or PpIX (60 nmoles) at 0.18 mol% PpIX-to-lipid ratio. Chloroform was removed via rotary evaporator overnight in order to create a thin film, which was rehydrated with 1 mL of deionized water. The lipid suspension was subjected to freeze-thaw cycles (4-45°C). The dispersions were extruded through polycarbonate membranes (0.1 μm pore size) at 42°C to form unilaminar vesicles. The final concentration of the dispersions was estimated by absorbance using the established molar extinction coefficient of BPD in DMSO ($\sim 34,895 \text{ M}^{-1}\text{cm}^{-1}$ at 687 nm) or PpIX in chloroform ($\sim 171,000 \text{ M}^{-1}\text{cm}^{-1}$ at 407 nm) or DMSO ($\sim 170,000 \text{ M}^{-1}\text{cm}^{-1}$ at 407 nm). The fluorescence-based optical characterization of Nal-BPD (Ex/Em: 435/600-800 nm) and Nal-PpIX (Ex/Em: 405/600-800 nm) was determined using a multi-mode microplate reader (Synergy Neo2; BioTek). NanoBrook Omni (Brookhaven) measured particle size and zeta potential. Nal-BPD and Nal-PpIX were diluted to 5 μM for all absorbance and fluorescence measurements in PBS, unless otherwise stated. Singlet oxygen production was monitored indirectly using the probe, SOSG. Within 96 well plates (black wall, transparent base) Nal-BPD or Nal-PpIX were mixed with SOSG (Thermo Fisher Scientific), to a final working solution of 0.5 μM of photosensitizer and 25 μM of SOSG in PBS. Samples were irradiated with 635 nm light (100 mW/cm^2) for Nal-PpIX and 690 nm light (100 mW/cm^2) for Nal-BPD, at different fluences of 0-80 J/cm^2 (ML6600 series laser module with 635 nm and 690 ± 5 nm lasers with 1.5 W output power each. SMA fiber output with SMA905 connector, Modulight). Fluorescence intensities of SOSG (Ex/Em: 504/525 nm) were acquired using a microplate reader (Synergy Neo2; BioTek) prior to and following irradiation.

Photobleaching of photosensitizers in ex vivo rat brains. Glass capillaries (300 μm in diameter; 1 cm in length) filled with 5 μM of Nal-BPD or Nal-PpIX were inserted in Sprague Dawley rat brains (Innovative Research) at varying depths (0-2 cm). Brain tissues (Innovative Research) were then exposed to surface illumination of red light (635 nm, for Nal-PpIX) or NIR light (690 nm, for Nal-BPD) at a fixed irradiance of 100 mW/cm^2 and with a range of fluences from 10-80 J/cm^2 using a diode laser (ML6600, Modulight). After light illumination, capillaries were removed, and the fluorescence emission from Nal-BPD (or Nal-PpIX) was measured by placing the capillaries on a flat black surface to minimize reflectance. Fluorescence images were acquired using a reflectance fluorescent microscope equipped with a 375 nm laser diode (L375P70MLD, Thorlabs). The light from the laser was then collimated, with 6 mW of light arriving on the sample. The emitted fluorescence and scattered light were then collected through another objective lens. The fluorescent and scattered light then passed through a filter (680-720 nm, Semrock). The remaining filtered fluorescent light was collected by a 12-bit CCD camera (EM-CCD, Cooke). All images were processed using ImageJ software (NIH).⁽⁸²⁾ Results are presented as mean \pm standard error of the mean (SEM). Statistical tests were carried out using GraphPad Prism. All experiments were carried out at least in triplicate.

RESULTS AND DISCUSSION

Synthesis and Characterization of Nal-BPD and Nal-PpIX

Nal-BPD and Nal-PpIX were reproducibly synthesized via the freeze-thaw extrusion method (42-45). A lipid composition of dipalmitoylphosphatidylcholine (DPPC), cholesterol, and distearoylphosphatidylethanolamine-methoxy polyethylene glycol (DSPE-PEG) at a 20:10:1 molar ratio was used based on the clinically approved PEGylated nanoliposomal formulations (46, 47). Here, both Nal-BPD and Nal-PpIX were grafted with 3 mol% of DSPE-PEG and formed in the size range of ~135-150 nm with a narrow size distribution (polydispersity index, $\text{PdI} < 0.1$). Cationic and unsaturated 1,2-dioleoyl-3-trimethylammonium-propane (DOTAP, 8 mol%) was introduced to the lipid composition to provide a neutral-to-positive zeta potential of +10-12 mV to balance toxicity, circulation, and tumor accumulation as described previously (47, 44, 48, 45). The incorporation of unsaturated lipids such as DOTAP could also accelerate light-triggered drug release via liposomal lipid oxidation as shown by others (49). In our study, photosensitizers (BPD or PpIX) were adsorbed in the liposomal

lipid-bilayer via hydrophobic and ionic interactions, resulting in an entrapment efficiency of $76.4 \pm 1.2\%$ and $44.9 \pm 0.7\%$ for Nal-BPD and Nal-PpIX, respectively (Table 1) (50). Our stability results suggest that 1-4 months of dark storage at 4°C and in phosphate-buffered saline (PBS) did not affect the overall size or monodispersity ($\text{PdI} < 0.1$) of Nal-BPD (139.7 ± 11.8 nm in diameter) and Nal-PpIX (150.9 ± 6.6 nm in diameter).

While nanoliposomes can maintain the stability and photoactivity of photosensitizers in biologically relevant media for effective PDT, hydrophobic photosensitizers in the lipid bilayer of liposomes are prone to quenching (51, 52, 50). To test if the unquenched photosensitizers (BPD or PpIX) are stabilized in the nanoliposomes and could be photo-activated for PDT, we evaluated the stability, quenching factor, and $^1\text{O}_2$ production of each photosensitizer in both free and nanoliposomal forms, with or without light activation. Changes in photosensitizer absorbance and fluorescence were monitored in dimethyl sulfoxide (DMSO) (Figures 1a, b) and in PBS (Figures 1c, d). In Figure 1c, the absorbance (blue dotted line) and fluorescence (red dotted line) spectra for free BPD in PBS were significantly lower than that of Nal-BPD (solid lines) in PBS, indicating the rapid aggregation of free BPD molecules under physiological conditions without being encapsulated in a nanoliposomal formulation. Similarly, 'recovery' of the absorbance (blue dotted line) and fluorescence (red dotted line) spectra of PpIX photosensitizers in PBS were made possible by the liposomal formulation (Figure 1d). These results suggest that the unquenched photosensitizers (BPD or PpIX) are stabilized in the nanoliposomes and could be activated by light for PDT, even without the release of photosensitizers from the nanoliposomes.

Light activation of photosensitizers could result in type I and/or type II reaction products (3). Under normoxic conditions, type II photosensitization is the dominant process in BPD-based PDT and PpIX-based PDT, which produce highly reactive $^1\text{O}_2$ that confers toxicity to nearby targets (3). It is well established that the $^1\text{O}_2$ quantum yield of BPD ($\Phi\Delta = 0.86$) is significantly higher than that of PpIX ($\Phi\Delta = 0.56$) (53-56). Here, using the Singlet Oxygen Sensor Green (SOSG) fluorescent probe, we test if 690 nm light activation of Nal-BPD could produce $^1\text{O}_2$ more efficiently in PBS, compared to 635 nm photo-activated Nal-PpIX. Upon light activation, the SOSG fluorescence intensity generated by Nal-BPD was markedly higher than that generated by Nal-PpIX, and in a light fluence dependent manner (Figure 2a). A plateau of SOSG fluorescence was observed at $80 \text{ J}/\text{cm}^2$, presumably due to an insufficient supply of oxygen or molecular probes. This data indicates that Nal-BPD produces $^1\text{O}_2$ more

efficiently than Nal-PpIX upon light activation under our experimental conditions. It is important to note that the higher $^1\text{O}_2$ production rate of Nal-BPD does not necessarily translate into more pronounced toxic effects, as the phototoxicity of the photosensitizer depends on the specific parameters involved, such as pharmacokinetics, biodistribution, cellular uptake, and subcellular targets of the photosensitizer, as well as the tumor microenvironment (3, 57, 2).

Evaluation of the Tissue-depth Dependent Photodynamic Effects of Nal-BPD and Nal-PpIX

Photobleaching is a process in which a photosensitizer (or fluorophore) permanently loses the ability to fluoresce and/or undergo type I/II reactions due to photochemical damage and covalent modification of the photosensitizer. Measuring the loss of fluorescence as the photosensitizer is photobleached is perhaps the most well studied and easily accessible tool for PDT monitoring and dosimetry in preclinical (Figure 2b) and clinical settings (58-61).

Here, we examined the penetration depth of the photodynamic effects in rat brains by monitoring the loss of fluorescence, as the photosensitizer is photobleached, after surface light illumination. Briefly, capillaries filled with 5 μM of Nal-BPD or Nal-PpIX, were inserted into the *ex vivo* rat brains at varying heights followed by surface illumination using appropriate wavelengths (i.e. 690 nm for Nal-BPD; 635 nm for Nal-PpIX) (Figure 3). After light activation, the total fluorescent signal was compared to a negative control to determine the degree of photobleaching. A non-linear decrease in the percentage of Nal-BPD (or Nal-PpIX) photobleaching was observed with increased tissue depth and reduced fluence (Figure 4a, b). Up to 10% photobleaching of Nal-BPD was observed at 1.4-2 cm (Figure 4a, c), while negligible (0-2%) photobleaching of Nal-PpIX was observed at 1 cm deep in brain tissue (Figure 4d). This result appears to be similar to previous findings (62, 63). Dereski and colleagues demonstrated that Photofrin[®], upon 632 nm light activation, induces a necrotic zone ~0.35 cm deep within male Fisher rat brains (62). A clinical study showed talaporfin, which is activated at a longer wavelength of 664 nm, could induce PDT damage (based on demyelination) up to 0.8 cm in a patient with recurrent glioma (63). It has also been shown that illumination geometry impacts the depth of brain tissue damage induced by PDT. Specifically, using hematoporphyrin derivative-based PDT, Perria et al. found that the depth of necrosis with surface illumination was 1.5 cm deep, compared with the 0.8 cm radius of cell killing found by Cheng et al. using an implanted optical fiber (22-24). Further studies

comparing surface illumination with illumination using implanted optical fibers are warranted.

In Figure 4a, b, we observed that the degree of photobleaching across different powers begins to converge as depth increases. This is because the loss of light intensity is non-linear. Simple 1-dimensional (1-D) modeling of light penetration has been described with the equation $\phi(z) = Eke^{-\mu z}$. (64) Where $\phi(z)$ is the fluence rate (W/cm^2) dependent on z , which is depth (cm). E is the irradiance delivered on the surface of the tissue (W/cm^2), k is backscattered light that augments irradiance on the surface of the tissue, and μ is the attenuation coefficient (cm^{-1}). Looking at the 1-D approximation, one important aspect to take note of is that the amount of energy lost in the tissue is dependent on e^{-z} , which shows an exponential decay in light intensity. Based on the above equation, it is expected that the photodynamic effect would be proportional to $\phi(z)$. Therefore, the degree of photobleaching versus the depth should have shown an exponential decay. Looking at Figure 4a, b this is not the exact case. Instead, the overall trend demonstrated was a plateau followed by an exponential decay. The main factors involved for the observed trend are due to the specular reflectance when the light hits the brain, and the boundary condition of the air-brain barrier.

Light scattering in tissue has been defined as being anisotropic, specifically regarding forward scattering. The magnitude of scattering is defined as g , with values being between -1 (back scattering) and 1 (forward scattering). Tissue is shown to have a g factor of 0.9, which means that while most light is forward scattering, some of the light is scattered back (65). Therefore, some light that has penetrated the tissue possesses the potential to be scattered back into the air. Air has been defined as having a refractive index of 1, while the brain has been defined to have a refractive index of 1.36 (66). The mismatch in refractive index results in some of the light that gets backscattered to the air-brain barrier getting reflected into the brain rather than escaping back into the air due to internal reflection. This is based on the angle at which the scattered light approaches the air-brain barrier. The angle at which light will be internally reflected is based off the equation $n_1 \sin(90) = n_2 \sin(\theta_c)$, where n_1 is the refractive index of air, n_2 is the refractive index of brain tissue, and θ_c is the critical angle. Therefore, any backscattered light that hits the air-brain barrier at a 47.3-degree angle will be reflected back into the brain. This coupled to the fact that a small amount of light gets reflected when the light first hits the brain signifies that for around 0-0.2 cm of the light

initially penetrating the brain, the fluence will increase slightly as depth increases (67-69). As the light penetrates farther into the brain, the light will start to demonstrate the typical exponential decay pattern. Due to the depth intervals taken, the photodynamic effect was not measured between 0-0.2 cm, meaning that the initial increase in fluorescence cannot be seen in Figure 4a, b. The effect instead manifests itself as an initial plateau, proceeded by an exponential decay.

PpIX demonstrating a shallower penetration depth compared to BPD is not all that surprising, even when PpIX is irradiated at two or three times the power compared to BPD. The main reason for this resides in the activation wavelength. BPD was activated using a 690 nm wavelength and PpIX was activated with a 630 nm wavelength. Although this is only a 60 nm shift, there is an appreciable drop in scattering and absorption by up to 40-50% (70-72). This led to the 690 nm light penetrating double the depth of the 630 nm light (73). The depth of treatment is described with the equation $z_{rx} = \delta \ln \left(\frac{Et\kappa}{H_{th}} \right)$. (68) z_{rx} is the depth penetration of the photodynamic effect, δ is optical penetration depth (cm), t is the exposure time (s), and H_{th} is the minimum amount of energy needed to make the photodynamic effect on the tissue ($W*s/cm^2$). Analysis of this equation reveals that increasing the E or t increases the depth of the effect by $\ln(Et)$, while increasing the wavelength would increase the optical penetration depth, which as a result would increase the penetration depth of the photodynamic effect in a proportional manner.

While Nal-BPD shows greater potential for depth penetration and production of 1O_2 in deeper tissue, Nal-PpIX still has high utility due to the ability to be used as a visual guide for tumor removal. Figure 5 shows a comparison of two capillary tubes. The top capillary was filled with Nal-BPD and the bottom capillary was filled with Nal-PpIX. Both samples were placed at similar heights, 0.04-0.05 cm below the surface of the brain. The images were taken with a phone camera (OnePlus 5). Inspection of the capillaries shows that PpIX fluorescence is more pronounced, this making it more easily visualized than Nal-BPD fluorescence. This is likely due to the higher fluorescence quantum yield of PpIX ($\Phi_F = 0.155$) and its fluorescence at 630 nm, while BPD fluoresces at 700 nm with a much lower fluorescence quantum yield ($\Phi_F = 0.051$) (53-56). Due to human spectral sensitivity, the emitted 630 nm light is seen with ten times greater sensitivity than the 690-710 nm light, allowing for enhanced visualization of PpIX even with the same amount of power being emitted (74).

In summary, the results show that the nanoliposomal formulations improve the stability and photoactivity of BPD and PpIX in biologically relevant media. Near-infrared (NIR) light (690 nm) activation of Nal-BPD induces $^1\text{O}_2$ production, which causes photobleaching of BPD up to 2 cm deep in brain tissues. In contrast, no photobleaching was observed beyond 1 cm deep in brain tissues upon red light (635 nm) activation of Nal-PpIX. The enhanced penetration depth of Nal-BPD-based PDT effects in the brain tissue paired with the use of Nal-PpIX for tumor visualization opens the door to developing and optimizing the combination of FGS and PDT for recurrent brain tumors, which typically occur within 1-2 centimeters of the original tumor (75-77). The data suggests that a strategic combination of FGS using PpIX, followed by PDT using BPD could take advantage of the strengths of both photosensitizers.

Combination treatments with two different photosensitizers have been shown to improve patient outcome. For example, in a clinical trial it was found that in patients with GBM, a combination treatment taking advantage of PpIX for FGS and Photofrin® to maximize tumor killing improved mean patient survival from 24.2 weeks to 52.8 weeks (12). BPD can treat areas deeper in the brain due to its longer emission wavelength and has the advantage of having a higher $^1\text{O}_2$ quantum yield compared to PpIX (78, 79). However, BPD can be difficult to visualize without additional instrumentation. PpIX does not suffer from this disadvantage and has been found to allow for accuracies up to 90% in differentiating tumor tissue from normal dura (80, 81). Characterization and optimization of Nal-PpIX-based FGS and Nal-BPD-based PDT in *ex vivo* brain tissues will pave the way towards investigating these new concepts in animals and eventually in patients.

Acknowledgements and Funding: This work is supported by the National Institutes of Health (NIH) R00 CA194269 grant (Huang), National Science Foundation CBET-1836740 (Chen), UMD start-up fund (Huang), and UMD-UMB 2018 Research and Innovation Seed Grant (Huang, Woodworth, and Chen). Mr. Brandon Gaitan is supported by the Clark Doctoral Fellowship Program.

REFERENCES

1. Yun, S. H. and S. J. J. Kwok (2017) Light in diagnosis, therapy and surgery. *Nature Biomedical Engineering* **1**, 0008.
2. Dolmans, D. E., D. Fukumura and R. K. Jain (2003) Photodynamic therapy for cancer. *Nat Rev Cancer* **3**, 380-387.
3. Celli, J. P., B. Q. Spring, I. Rizvi, C. L. Evans, K. S. Samkoe, S. Verma, B. W. Pogue and T. Hasan (2010) Imaging and photodynamic therapy: mechanisms, monitoring, and optimization. *Chem Rev* **110**, 2795-2838.
4. Huang, H. C. and T. Hasan (2014) The “Nano” World in Photodynamic Therapy *Austin J Nanomed Nanotechnol* **2**, 1020.
5. Obaid, G., M. Broekgaarden, A.-L. Bulin, H.-C. Huang, J. Kuriakose, J. Liu and T. Hasan (2016) Photonanomedicine: a convergence of photodynamic therapy and nanotechnology. *Nanoscale* **8**, 12471-12503.
6. Stummer, W., U. Pichlmeier, T. Meinel, O. D. Wiestler, F. Zanella and H. J. Reulen (2006) Fluorescence-guided surgery with 5-aminolevulinic acid for resection of malignant glioma: a randomised controlled multicentre phase III trial. *Lancet Oncol* **7**, 392-401.
7. Bechet, D., S. R. Mordon, F. Guillemain and M. A. Barberi-Heyob (2014) Photodynamic therapy of malignant brain tumours: A complementary approach to conventional therapies. *Cancer Treatment Reviews* **40**, 229-241.
8. Lakomkin, N. and C. G. Hadjipanayis (2018) Fluorescence-guided surgery for high-grade gliomas. *Journal of surgical oncology* **118**, 356-361.
9. Hadjipanayis, C. G. and W. Stummer (2019) 5-ALA and FDA approval for glioma surgery. *Journal of neuro-oncology* **141**, 479-486.
10. Ostrom, Q. T., H. Gittleman, P. Liao, T. Vecchione-Koval, Y. Wolinsky, C. Kruchko and J. S. Barnholtz-Sloan (2017) CBTRUS Statistical Report: Primary brain and other central nervous system tumors diagnosed in the United States in 2010-2014. *Neuro Oncol* **19**, v1-v88.
11. Kostron, H., A. Obwegeser and R. Jakober (1996) Photodynamic therapy in neurosurgery: a review. *J Photochem Photobiol B* **36**, 157-168.
12. Eljamel, M. S., C. Goodman and H. Moseley (2008) ALA and Photofrin fluorescence-guided resection and repetitive PDT in glioblastoma multiforme: a single centre Phase III randomised controlled trial. *Lasers Med Sci* **23**, 361-367.
13. Dupont, C., M. Vermandel, H. A. Leroy, M. Quidet, F. Lecomte, N. Delhem, S. Mordon and N. Reyns (2019) INtraoperative photoDYnamic Therapy for GliOblastomas (INDYGO): Study Protocol for a Phase I Clinical Trial. *Neurosurgery* **84**, E414-e419.
14. Sandell, J. L. and T. C. Zhu (2011) A review of in-vivo optical properties of human tissues and its impact on PDT. *Journal of biophotonics* **4**, 773-787.
15. Wang, P. and T. Li (2019) Which wavelength is optimal for transcranial low-level laser stimulation? *Journal of biophotonics* **12**, e201800173.
16. Li, T., C. Xue, P. Wang, Y. Li and L. Wu (2017) Photon penetration depth in human brain for light stimulation and treatment: A realistic Monte Carlo simulation study. *Journal of Innovative Optical Health Sciences* **10**, 1743002.
17. Haeussinger, F. B., S. Heinzl, T. Hahn, M. Schecklmann, A. C. Ehlis and A. J. Fallgatter (2011) Simulation of near-infrared light absorption considering individual head and prefrontal cortex anatomy: implications for optical neuroimaging. *PLoS One* **6**, e26377.

18. Pitzschke, A., B. Lovisa, O. Seydoux, M. Zellweger, M. Pfeleiderer, Y. Tardy and G. Wagnieres (2015) Red and NIR light dosimetry in the human deep brain. *Physics in medicine and biology* **60**, 2921-2937.
19. Tedford, C. E., S. DeLapp, S. Jacques and J. Anders (2015) Quantitative analysis of transcranial and intraparenchymal light penetration in human cadaver brain tissue. *Lasers Surg Med* **47**, 312-322.
20. Henderson, T. A. and L. D. Morries (2015) Near-infrared photonic energy penetration: can infrared phototherapy effectively reach the human brain? *Neuropsychiatric disease and treatment* **11**, 2191-2208.
21. Hamblin, M. R. (2016) Shining light on the head: Photobiomodulation for brain disorders. *BBA clinical* **6**, 113-124.
22. Perria, C., T. Capuzzo, G. Cavagnaro, R. Datti, N. Francaviglia, C. Rivano and V. E. Tercero (1980) Fast attempts at the photodynamic treatment of human gliomas. *Journal of neurosurgical sciences* **24**, 119-129.
23. Cheng, M., J. McKean, D. Boisvert, J. Tulip and M. W.B. (1984) Effects of Photoradiation Therapy on Normal Rat Brain. *Neurosurgery* **15**, 804-810.
24. Wilson, B. C., P. J. Muller and J. C. Yanch (1986) Instrumentation and light dosimetry for intra-operative photodynamic therapy (PDT) of malignant brain tumours. *Physics in medicine and biology* **31**, 125-133.
25. Olzowy, B., C. S. Hundt, S. Stocker, K. Bise, H. J. Reulen and W. Stummer (2002) Photoirradiation therapy of experimental malignant glioma with 5-aminolevulinic acid. *Journal of neurosurgery* **97**, 970-976.
26. Shackley, D. C., C. Whitehurst, J. V. Moore, N. J. George, C. D. Betts and N. W. Clarke (2000) Light penetration in bladder tissue: implications for the intravesical photodynamic therapy of bladder tumours. *BJU international* **86**, 638-643.
27. Huang, H. C., S. Mallidi, G. Obaid, B. Sears, S. Tangutoori and T. Hasan (2015) 23 - Advancing photodynamic therapy with biochemically tuned liposomal nanotechnologies. In *Applications of Nanoscience in Photomedicine*. (Edited by M. R. Hamblin and P. Avci), pp. 487-510. Chandos Publishing, Oxford.
28. (1999) Photodynamic therapy of subfoveal choroidal neovascularization in age-related macular degeneration with verteporfin: one-year results of 2 randomized clinical trials--TAP report. Treatment of age-related macular degeneration with photodynamic therapy (TAP) Study Group. *Archives of ophthalmology (Chicago, Ill. : 1960)* **117**, 1329-1345.
29. Schmidt-Erfurth, U., T. Hasan, E. Gragoudas, N. Michaud, T. J. Flotte and R. Birngruber (1994) Vascular targeting in photodynamic occlusion of subretinal vessels. *Ophthalmology* **101**, 1953-1961.
30. Schmidt, M. H., G. A. Meyer, K. W. Reichert, J. Cheng, H. G. Krouwer, K. Ozker and H. T. Whelan (2004) Evaluation of photodynamic therapy near functional brain tissue in patients with recurrent brain tumors. *Journal of neuro-oncology* **67**, 201-207.
31. Wachowska, M., A. Muchowicz, M. Firczuk, M. Gabrysiak, M. Winiarska, M. Wańczyk, K. Bojarczuk and J. Golab *Aminolevulinic Acid (ALA) as a Prodrug in Photodynamic Therapy of Cancer*. *Molecules*. 2011 May 19;16(5):4140-64. doi: 10.3390/molecules16054140. eCollection 2011 May.
32. Rück, A. and R. Steiner (1998) Basic reaction mechanisms of hydrophilic and lipophilic photosensitisers in photodynamic tumour treatment. *Minimally Invasive Therapy & Allied Technologies* **7**, 503-509.
33. Harmatys, K. M., A. J. Musso, K. J. Clear and B. D. Smith (2016) Small molecule additive enhances cell uptake of 5-aminolevulinic acid and conversion to protoporphyrin IX. *Photochemical & photobiological sciences : Official journal of*

the European Photochemistry Association and the European Society for Photobiology **15**, 1408-1416.

34. Utsuki, S., H. Oka, S. Sato, S. Shimizu, S. Suzuki, Y. Tanizaki, K. Kondo, Y. Miyajima and K. Fujii (2007) Histological examination of false positive tissue resection using 5-aminolevulinic acid-induced fluorescence guidance. *Neurol Med Chir (Tokyo)* **47**, 210-213; discussion 213-214.
35. Ding, H., B. D. Sumer, C. W. Kessinger, Y. Dong, G. Huang, D. A. Boothman and J. Gao (2011) Nanoscopic micelle delivery improves the photophysical properties and efficacy of photodynamic therapy of protoporphyrin IX. *Journal of controlled release : official journal of the Controlled Release Society* **151**, 271-277.
36. Manivasager, V., K. K. Yee, P. W. Heng, K. C. Soo and M. Olivo (2006) A study comparing endogenous protoporphyrin IX induced by 5-ALA and ALA-methyl ester with exogenous PpIX and PpIX dimethyl ester in photodynamic diagnosis of human nasopharyngeal carcinoma xenografts. *International journal of oncology* **29**, 997-1002.
37. Tachikawa, S., S. Sato, H. Hazama, Y. Kaneda, K. Awazu and H. Nakamura (2015) Localization-dependent cell-killing effects of protoporphyrin (PPIX)-lipid micelles and liposomes in photodynamic therapy. *Bioorganic & medicinal chemistry* **23**, 7578-7584.
38. Zou, X., M. Yao, L. Ma, M. Hossu, X. Han, P. Juzenas and W. Chen (2014) X-ray-induced nanoparticle-based photodynamic therapy of cancer. *Nanomedicine (London, England)* **9**, 2339-2351.
39. Yan, L., A. Amirshaghghi, D. Huang, J. Miller, J. M. Stein, T. M. Busch, Z. Cheng and A. Tsourkas (2018) Protoporphyrin IX (PpIX)-Coated Superparamagnetic Iron Oxide Nanoparticle (SPION) Nanoclusters for Magnetic Resonance Imaging and Photodynamic Therapy. *Adv Funct Mater* **28**, 1707030.
40. Stummer, W., S. Stocker, S. Wagner, H. Stepp, C. Fritsch, C. Goetz, A. E. Goetz, R. Kiefmann and H. J. Reulen (1998) Intraoperative detection of malignant gliomas by 5-aminolevulinic acid-induced porphyrin fluorescence. *Neurosurgery* **42**, 518-525; discussion 525-516.
41. Kaneko, S. and S. Kaneko (2016) Fluorescence-Guided Resection of Malignant Glioma with 5-ALA. *Int J Biomed Imaging* **2016**, 6135293-6135293.
42. Baglo, Y., B. J. Liang, R. W. Robey, S. V. Ambudkar, M. M. Gottesman and H.-C. Huang (2019) Porphyrin-lipid assemblies and nanovesicles overcome ABC transporter-mediated photodynamic therapy resistance in cancer cells. *Cancer Letters* **457**, 110-118.
43. Pigula, M., H. C. Huang, S. Mallidi, S. Anbil, J. Liu, Z. Mai and T. Hasan (2018) Size-dependent Tumor Response to Photodynamic Therapy and Irinotecan Monotherapies Revealed by Longitudinal Ultrasound Monitoring in an Orthotopic Pancreatic Cancer Model. *Photochem Photobiol.*
44. Huang, H. C., I. Rizvi, J. Liu, S. Anbil, A. Kalra, H. Lee, Y. Baglo, N. Paz, D. Hayden, S. Pereira, B. W. Pogue, J. Fitzgerald and T. Hasan (2018) Photodynamic Priming Mitigates Chemotherapeutic Selection Pressures and Improves Drug Delivery. *Cancer Res* **78**, 558-571.
45. Huang, H. C., S. Mallidi, J. Liu, C. T. Chiang, Z. Mai, R. Goldschmidt, N. Ebrahim-Zadeh, I. Rizvi and T. Hasan (2016) Photodynamic Therapy Synergizes with Irinotecan to Overcome Compensatory Mechanisms and Improve Treatment Outcomes in Pancreatic Cancer. *Cancer Res* **76**, 1066-1077.

46. Chang, H. I. and M. K. Yeh (2012) Clinical development of liposome-based drugs: formulation, characterization, and therapeutic efficacy. *International journal of nanomedicine* **7**, 49-60.
47. Torchilin, V. P. (2005) Recent advances with liposomes as pharmaceutical carriers. *Nature reviews. Drug discovery* **4**, 145-160.
48. Huang, H. C., J. Liu, Y. Baglo, I. Rizvi, S. Anbil, M. Pigula and T. Hasan (2018) Mechanism-informed Repurposing of Minocycline Overcomes Resistance to Topoisomerase Inhibition for Peritoneal Carcinomatosis. *Molecular cancer therapeutics* **17**, 508-520.
49. Miranda, D. and J. F. Lovell (2016) Mechanisms of Light-induced Liposome Permeabilization. *Bioeng Transl Med* **1**, 267-276.
50. Chowdhary, R. K., I. Shariff and D. Dolphin (2003) Drug release characteristics of lipid based benzoporphyrin derivative. *Journal of pharmacy & pharmaceutical sciences : a publication of the Canadian Society for Pharmaceutical Sciences, Societe canadienne des sciences pharmaceutiques* **6**, 13-19.
51. Kachatkou, D., S. Sasnouski, V. Zorin, T. Zorina, M. A. D'Hallewin, F. Guillemain and L. Bezdetnaya (2009) Unusual photoinduced response of mTHPC liposomal formulation (Foslip). *Photochemistry and photobiology* **85**, 719-724.
52. Lovell, J. F., C. S. Jin, E. Huynh, H. Jin, C. Kim, J. L. Rubinstein, W. C. Chan, W. Cao, L. V. Wang and G. Zheng (2011) Porphysome nanovesicles generated by porphyrin bilayers for use as multimodal biophotonic contrast agents. *Nature materials* **10**, 324-332.
53. Aveline, B. M., T. Hasan and R. W. Redmond (1995) The effects of aggregation, protein binding and cellular incorporation on the photophysical properties of benzoporphyrin derivative monoacid ring A (BPDMA). *J Photochem Photobiol B* **30**, 161-169.
54. Redmond, R. W. and J. N. Gamlin (1999) A compilation of singlet oxygen yields from biologically relevant molecules. *Photochem Photobiol* **70**, 391-475.
55. Aveline, B., T. Hasan and R. W. Redmond (1994) Photophysical and photosensitizing properties of benzoporphyrin derivative monoacid ring A (BPD-MA). *Photochem Photobiol* **59**, 328-335.
56. Lozovaya, G. I., Z. Masinovsky and A. A. Sivash (1990) Protoporphyrin ix as a possible ancient photosensitizer: Spectral and photochemical studies. *Origins of life and evolution of the biosphere* **20**, 321-330.
57. Castano, A. P., P. Mroz and M. R. Hamblin (2006) Photodynamic therapy and anti-tumour immunity. *Nat Rev Cancer* **6**, 535-545.
58. Jarvi, M. T., M. S. Patterson and B. C. Wilson (2012) Insights into photodynamic therapy dosimetry: simultaneous singlet oxygen luminescence and photosensitizer photobleaching measurements. *Biophysical journal* **102**, 661-671.
59. Kim, M. M., J. C. Finlay and T. C. Zhu (2015) Macroscopic singlet oxygen model incorporating photobleaching as an input parameter. *Proceedings of SPIE--the International Society for Optical Engineering* **9308**, 93080v.
60. Finlay, J. C., S. Mitra and T. H. Foster (2002) In vivo mTHPC photobleaching in normal rat skin exhibits unique irradiance-dependent features. *Photochem Photobiol* **75**, 282-288.
61. Finlay, J. C., S. Mitra, M. S. Patterson and T. H. Foster (2004) Photobleaching kinetics of Photofrin in vivo and in multicell tumour spheroids indicate two simultaneous bleaching mechanisms. *Physics in medicine and biology* **49**, 4837-4860.
62. Dereski, M. O., M. Chopp, J. H. Garcia and F. W. Hetzel (1991) Depth measurements and histopathological characterization of photodynamic therapy generated normal

- brain necrosis as a function of incident optical energy dose. *Photochem Photobiol* **54**, 109-112.
63. Ikuta, S., Y. Kawase, Y. Muragaki, T. Maruyama, M. Nitta, T. Saito and H. Iseki (2015) Penetration depth of the 664-nm semiconductor laser light with talaporfin sodium into human brain tissue with glioma. *Photodiagnosis and Photodynamic Therapy* **12**, 349.
64. Jacques, S. L. (1992) *Simple optical theory for light dosimetry during PDT (Invited Paper)*. SPIE.
65. Jacques, S. L. (2013) Optical properties of biological tissues: a review. *Physics in medicine and biology* **58**, R37-R61.
66. Binding, J., J. Ben Arous, J. F. Leger, S. Gigan, C. Boccara and L. Bourdieu (2011) Brain refractive index measured in vivo with high-NA defocus-corrected full-field OCT and consequences for two-photon microscopy. *Optics express* **19**, 4833-4847.
67. Jacques, S. L. (1998) Light distributions from point, line and plane sources for photochemical reactions and fluorescence in turbid biological tissues. *Photochem Photobiol* **67**, 23-32.
68. Jacques, S. L. (2010) How tissue optics affect dosimetry of photodynamic therapy. *J Biomed Opt* **15**, 051608.
69. Ong, Y. H. and T. C. Zhu (2016) Analytic function for predicting light fluence rate of circular fields on a semi-infinite turbid medium. *Optics express* **24**, 26261-26281.
70. Bevilacqua, F., D. Piguet, P. Marquet, J. D. Gross, B. J. Tromberg and C. Depeursinge (1999) In vivo local determination of tissue optical properties: applications to human brain. *Applied optics* **38**, 4939-4950.
71. Yona, G., N. Meitav, I. Kahn and S. Shoham (2016) Realistic Numerical and Analytical Modeling of Light Scattering in Brain Tissue for Optogenetic Applications. *eneuro* **3**, ENEURO.0059-0015.2015.
72. Josefsen, L. B. and R. W. Boyle (2008) Photodynamic therapy and the development of metal-based photosensitisers. *Metal-based drugs* **2008**, 276109.
73. Hart, N. S. and M. Fitzgerald (2016) A new perspective on delivery of red-near-infrared light therapy for disorders of the brain. *Discovery medicine* **22**, 147-156.
74. Schnapf, J. L., T. W. Kraft and D. A. Baylor (1987) Spectral sensitivity of human cone photoreceptors. *Nature* **325**, 439-441.
75. Wallner, K. E., J. H. Galicich, G. Krol, E. Arbit and M. G. Malkin (1989) Patterns of failure following treatment for glioblastoma multiforme and anaplastic astrocytoma. *Int J Radiat Oncol Biol Phys* **16**, 1405-1409.
76. Sherriff, J., J. Tamangani, L. Senthil, G. Cruickshank, D. Spooner, B. Jones, C. Brookes and P. Sanghera (2013) Patterns of relapse in glioblastoma multiforme following concomitant chemoradiotherapy with temozolomide. *The British Journal of Radiology* **86**, 20120414.
77. Silbergeld, D. L. and M. R. Chicoine (1997) Isolation and characterization of human malignant glioma cells from histologically normal brain. *Journal of neurosurgery* **86**, 525-531.
78. Simone, C. B., 2nd, J. S. Friedberg, E. Glatstein, J. P. Stevenson, D. H. Serman, S. M. Hahn and K. A. Cengel (2012) Photodynamic therapy for the treatment of non-small cell lung cancer. *Journal of thoracic disease* **4**, 63-75.
79. Zhu, T. C., B. Liu, M. M. Kim, D. McMillan, X. Liang, J. C. Finlay and T. M. Busch (2014) Comparison of singlet oxygen threshold dose for PDT. *Proceedings of SPIE--the International Society for Optical Engineering* **8931**.
80. Valdes, P. A., K. Bekelis, B. T. Harris, B. C. Wilson, F. Leblond, A. Kim, N. E. Simmons, K. Erkmens, K. D. Paulsen and D. W. Roberts (2014) 5-Aminolevulinic acid-induced protoporphyrin IX fluorescence in meningioma: qualitative and

quantitative measurements in vivo. *Neurosurgery* **10 Suppl 1**, 74-82; discussion 82-73.

81. Haar, C. P., P. Hebbar, G. C. t. Wallace, A. Das, W. A. Vandergrift, 3rd, J. A. Smith, P. Giglio, S. J. Patel, S. K. Ray and N. L. Banik (2012) Drug resistance in glioblastoma: a mini review. *Neurochemical research* **37**, 1192-1200.

82. Schneider, C. A., W. S. Rasband and K. W. Eliceiri (2012) NIH Image to ImageJ: 25 years of image analysis. *Nat Methods* **9**, 671-675.

Table 1. Overview of the characterization of Nal-BPD and Nal-PpIX detailing their respective hydrodynamic diameter, polydispersity index, zeta potential, entrapment efficiency, and loading capacity. Values are presented as mean \pm SEM.

Parameters \ Photosensitizer	Nal-BPD	Nal-PpIX
Hydrodynamic diameter (nm)	135.7 \pm 8.0	153.1 \pm 4.9
Polydispersity index (PdI)	0.06 \pm 0.02	0.04 \pm 0.02
Zeta potential (mV)	10.1 \pm 1.2	12.4 \pm 1.8
Entrapment efficiency* (%)	76.4 \pm 1.2	44.9 \pm 0.7
Loading capacity** (%)	0.117 \pm 0.002	0.065 \pm 0.001

* The molar ratio of drug entrapped within the nanoliposome to the total drug added initially.

** The ratio of final photosensitizer *wt.* to the overall *wt.* of the nanoliposomes.

FIGURE CAPTIONS

Figure 1. Absorbance (blue) and fluorescence (red) spectra of BPD, PpIX, Nal-BPD, and Nal-PpIX. (a) Free form BPD fully dissolved in DMSO has a strong absorbance peak at 435 nm (Soret band) and 690 nm (Q band). Typically, 690 nm light is applied to activate BPD for PDT. Fluorescent BPD has a peak emission in the NIR range (λ_{max} at \sim 700 nm). (b) Free form PpIX fully dissolved in DMSO shows a strong absorbance peak at 405 nm (Soret band), with multiple Q bands in the green to red range. Typically, PpIX is activated by 635 nm light or 375-440 nm light for PDT or FGS, respectively. The fluorescence signal emitted by PpIX is in the red/NIR range between 635 and 700 nm. (c) Free BPD is hydrophobic and readily aggregates in PBS, as demonstrated by the decrease in magnitude of the absorbance spectrum, resulting in fluorescence quenching of BPD with minimal photoactivity ($<$ 2%). Entrapping BPD in a nanoliposomal formulation restores its fluorescence and photoactivity ($35.8 \pm 0.2\%$) in PBS. (d) Likewise, free form PpIX aggregates in PBS, leading to a

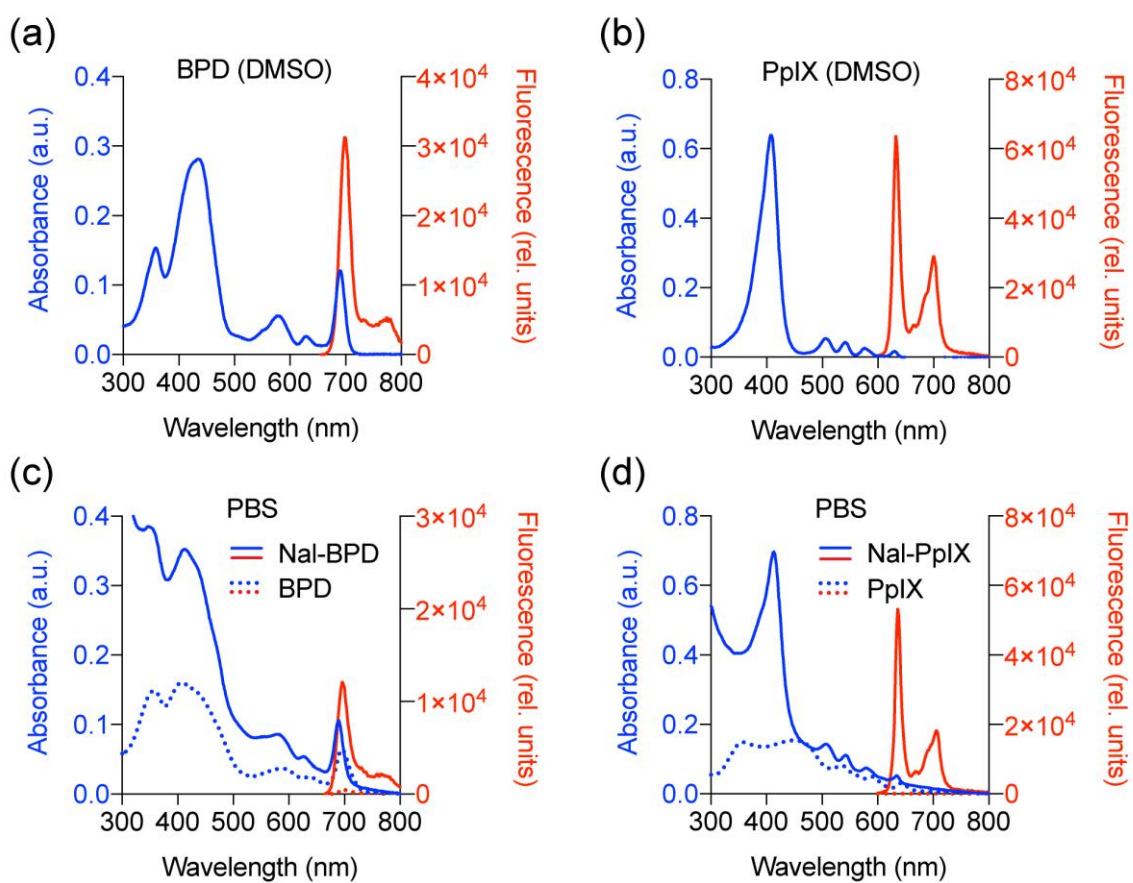
quenched state that is no longer activatable at 635 nm. Similarly, the encapsulation of PpIX within a nanoliposomal formulation restores its fluorescence and photoactivity up to $82.8 \pm 0.1\%$.

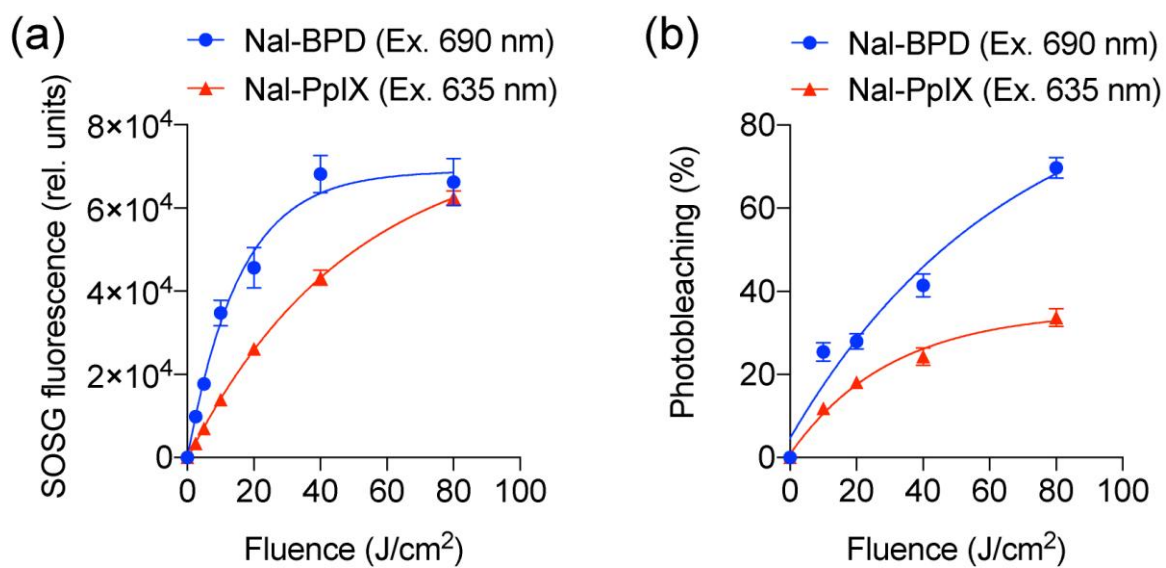
Figure 2. Singlet oxygen ($^1\text{O}_2$) production and photobleaching of Nal-BPD and Nal-PpIX upon light activation. (a) SOSG fluorescence emission and (b) photobleaching percentage of Nal-BPD and Nal-PpIX with respect to increasing fluences of light at 690 nm and 635 nm, respectively.

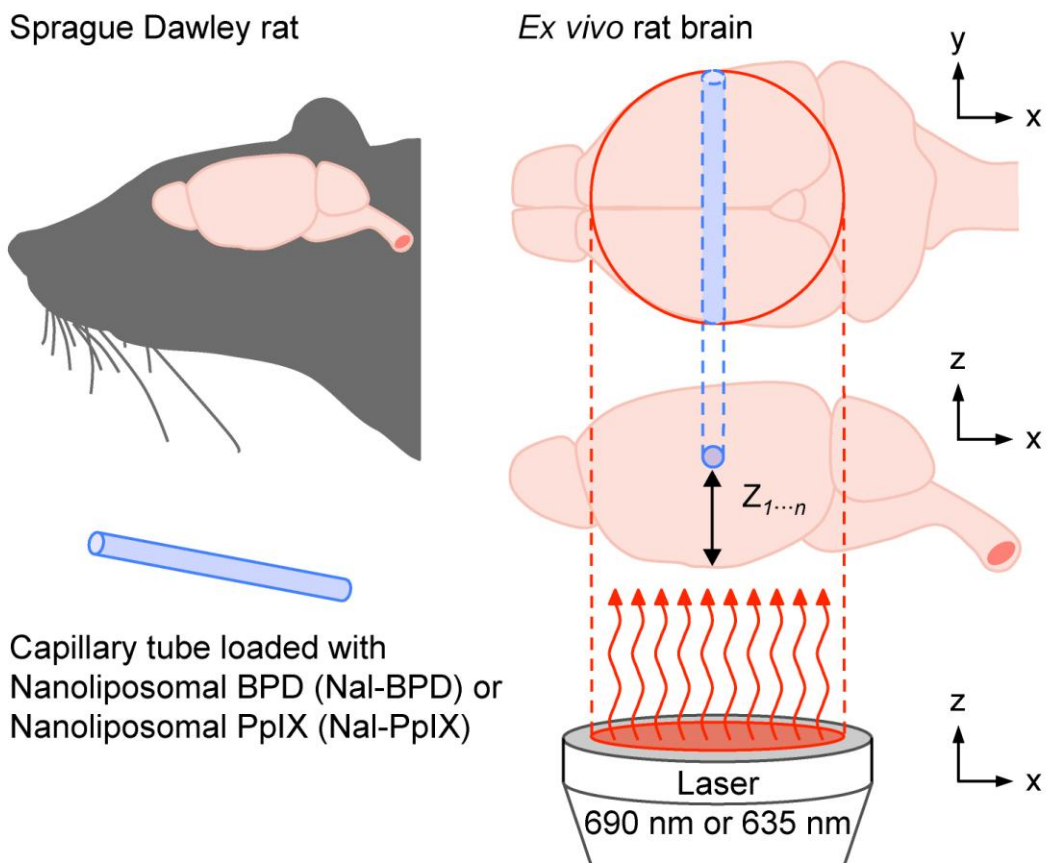
Figure 3. Experimental setup for examining the limit of the photodynamic effect. Glass capillaries filled with $5 \mu\text{M}$ of Nal-BPD or Nal-PpIX were inserted at various heights (Z, cm) in Sprague Dawley rat brains and exposed to surface illumination of 690 nm or 635 nm at various fluences.

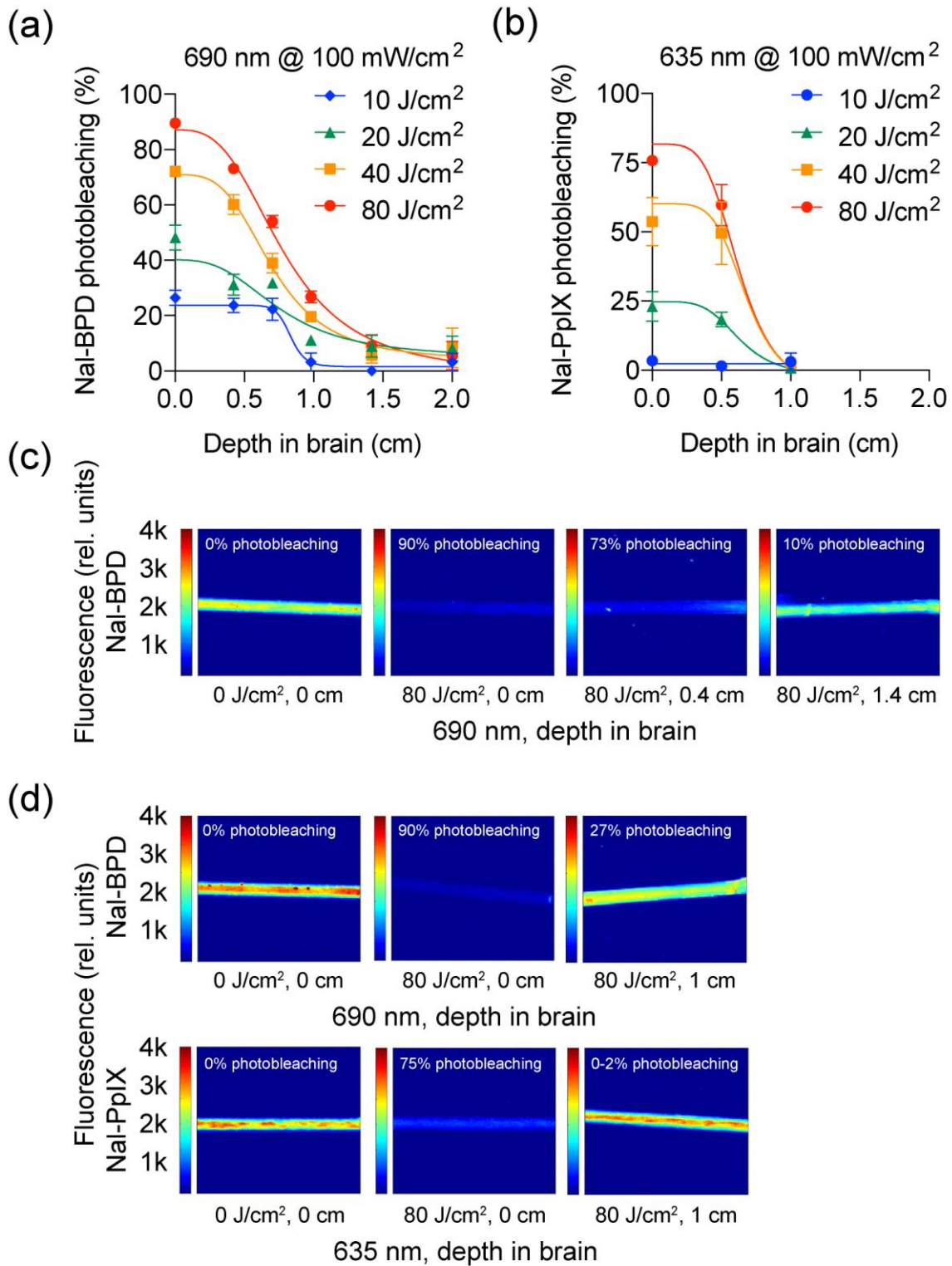
Figure 4. Depth of photosensitizer activation within brain tissue determined via degree of photobleaching. Glass capillaries ($300 \mu\text{m}$ in diameter) containing $5 \mu\text{M}$ of Nal-BPD (or Nal-PpIX) were inserted at varying depths within *ex vivo* rat brains and irradiated with light (690 nm or 635 nm; $100 \text{ mW}/\text{cm}^2$; 0, 10, 20, 40, $80 \text{ J}/\text{cm}^2$). Photobleaching of (a) Nal-BPD and (b) Nal-PpIX were evaluated at different depths and fluences. (c) Fluorescence images of capillaries filled with Nal-BPD showing 90, 73, and 10% photobleaching in brain tissues at 0, 0.4, and 1.4 cm deep, respectively. (d) At $80 \text{ J}/\text{cm}^2$, 27% Nal-BPD photobleaching was observed 1 cm deep in tissue, in contrast to only 0-2% photobleaching of Nal-PpIX.

Figure 5. Visualization of the fluorescent emission of Nal-BPD and Nal-PpIX when excited at 375 nm. (a) Capillaries ($300 \mu\text{m}$ in diameter) filled with the photosensitizers (Nal-BPD or Nal-PpIX, $5 \mu\text{M}$) were excited with 375 nm and captured with a phone camera (OnePlus 5). PpIX's fluorescent signal can be easily visualized by the naked eye. (b) Capillaries were inserted into the brain and were excited to examine if the fluorescent signal could be visualized through brain tissue. The emission signal from PpIX could be seen when the capillary was inserted $\sim 0.04\text{-}0.05$ cm deep in tissue (black arrow).

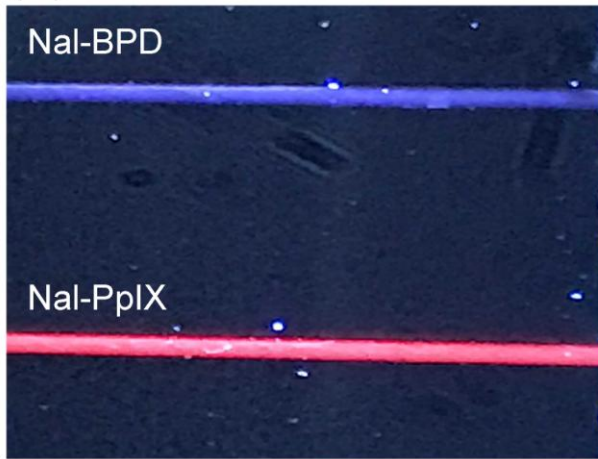








(a)



(b)

